High-temperature and High-pressure Sintering Method to Prepare Magnetite Reference Material for In-situ Microanalysis

Xiao-Wen Huang, [a] Yu-Miao Meng,[a] Sen Lin, [b,*] and Liang Qi [a]

[a] State Key Laboratory of Ore Deposit Geochemistry, Institute of Geochemistry, Chinese Academy of Sciences, Guiyang 550081, China

[b] Key Laboratory for High Temperature and High Pressure Study of the Earth's Interior, Institute of Geochemistry, Chinese Academy of Sciences, Guiyang 550081, China

ABSTRACT: Matrix-matched reference materials are important for in situ trace and isotope analyses. In this study, we developed an efficient method for preparing chemically homogeneous magnetite (MtTR-1) without adding a binder. The initial magnetite powder (d_{90} = ~80 μm) was milled to form micron (d_{90} = 3.0 μm) particles in an anhydrous ethanol suspension and argon environment using a high-energy vibration ball mill. The obtained particles were pressed into a magnetite cylinder (10 mm in diameter and 9.2 mm in height), sealed into a silver tube, and sintered at 500 °C and 1.2 GPa for 2 h. Laser Raman spectroscopy results indicated that high-temperature and high-pressure sintering did not induce any phase transformation. The smooth surface after polishing was subjected to repeated analyses via electron probe microanalyzer using a spot size of 5 μm and laser ablation-inductively coupled plasma-mass spectrometry (LA-ICP-MS) using spot sizes of 38-60 μm. The results indicated that the texture and chemical composition are homogeneous in MtTR-1. The smooth time-resolved signal intensities of elements, steep wall, and flat bottom of ablation craters also suggested homogeneity in the depth profile. Line profile analyses across the entire pressed pellet further demonstrated that the pellet is homogenous for the investigated elements. The concentrations of major and trace elements in MtTR-1 determined by ICP-OES and ICP-MS are used as the preferred values. The MtTR-1 can be cut into slices, repeatedly polished and used for in situ analyses. The proposed technique for producing magnetite can also be applicable to other minerals or rocks by optimizing the conditions, thus providing a new method for preparing reference materials for in-situ microanalysis.
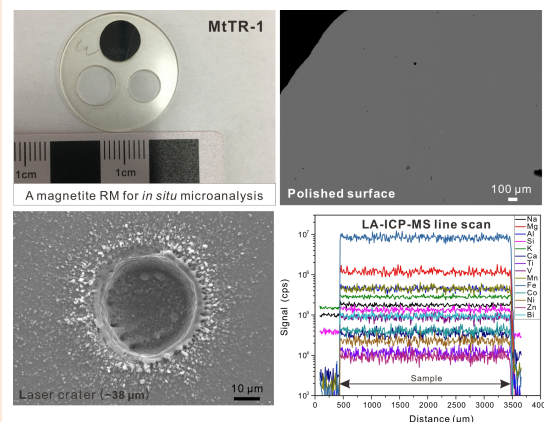
INTRODUCTION

Magnetite (Fe_3O_4) has an inverse spinel structure and contains many minor and trace elements, such as Mg, Al, Si, Ca, Ti, V, Mn, Cr, and Ni. Trace elements in magnetite have been widely used in petrogenesis and ore genesis studies.[1-4] Laser ablation-inductively coupled plasma-mass spectrometry (LA-ICP-MS) is a commonly used technique for determining trace elements in minerals, such as magnetite, because of its low detection limit down to pg g^{-1} level and high spatial resolution of a few to tens of micrometers.[5-7] Because of the lack of matrix-matched magnetite reference materials (RMs) for in situ trace element analysis, the existing methods use National Institute of Standards and Technology (NIST)-series RMs such as NIST 610 and NIST 2782,[8,9] United States Geological Survey (USGS) RMs such as GSE-1G, BCR-2G, BHVO-2G, and BIR-1G, and the newly developed andesitic glass reference materials (ARM-1, -2, -3) as the external calibration standard,[10-16] and both NIST-series and USGS RMs.[17,18] Although different methods for determining trace elements in magnetite have been established,[8-14] comparative studies between them are inadequate because of the lack of matrix-matched magnetite RMs for quality control purpose.

The reliability of the LA-ICP-MS method for determination of trace elements in magnetite is commonly verified by Fe-rich glasses (GSD-1G, ARM-1 and GOR-128G)[10,16] and the natural magnetite (BC-28, from the Bushveld Complex).[18,19] Natural magmatic magnetite, BC-28, contains limited number of elements with reference values, including Mg, Al, Sc, Ti, V, Cr, Mn, Co, Ni, Cu, and Zn.[18] Several elements including Cu and Ti show heterogeneity in this sample.[14] Moreover, minor amounts of mineral inclusions are inevitable in nature magnetite. Therefore, it is necessary to develop magnetite with a homogeneous composition that contains more elements with reference values.

There are four common methods to develop RMs for in situ microanalysis: synthesis of minerals by crystal growth, selection of homogeneous natural minerals, fusion, and pressed powder tablets (PPTs). For the PPT, the rock or mineral powders are ground to micron or nanometer scales, mixed with or without a binder, and pressed under a specific pressure and temperature condition. The PPT method is commonly used for sample preparation in X-ray fluorescence analysis[20] and was introduced for LA-ICP-MS by Gray.[21] Numerous studies have discussed the effects of the grain size, milling method, pressure, and binder type on the results of PPT preparation.[22-25] The effect of different analytical conditions of LA-ICP-MS was also investigated to obtain better results.[23] The sample homogeneity and stability were strongly dependent on the grain size of the powder, and particles on the nanoscale (*e.g.*, $d_{90} = 7.9$ μm) yielded a homogeneous signal during ICP-MS analysis.[22] To obtain nanoscale particles, wet milling is more effective than dry milling.[22] The pressure for PPT preparation commonly ranges from 200 to 700 MPa and the temperature is room temperature.[22,23,26] High-temperature and high-pressure sintering have also been reported for preparing RMs.[27-29] A platinum-group-element-based sulfide RM was prepared by sintering sulfides at 900–1200°C and 1.5–2 GPa.[28] Sintering nanocrystalline calcite at high temperature (1000 °C) and high pressure (1 GPa) to prepare calcite for secondary ion mass spectrometry oxygen isotope analysis has also been reported,[29] however, the grain size of homogeneous calcite is only 100–500 μm. In addition to the conditions for sintering, the types of binders were also evaluated. A series of materials including cellulose,[30,31] vanillic acid, pyrazinoic acid, and nicotinic acid,[32] synthetic resins,[33,34] zinc-oxide-eugenol complex,[35] and polyvinyl alcohol[23] have been used as binders. Because of the possible contamination from binders, particularly during trace element analysis, preparing PPT without adding a binder is also favorable.[22,36,37] As discussed above, methods for preparing RMs for trace element analysis of different types of rocks and minerals such as calcite and sulfides have been reported. However, no detailed method for sintering magnetite RMs was reported so far.

In this study, we developed a novel technique for synthesizing magnetite (MtTR-1) using a submicron-scale powder of natural magnetite under high-temperature (500 °C) and high-pressure (1.2 GPa) conditions. During sintering, the original chemical composition and crystal structure of the magnetite particles were retained, and the density of the synthesized magnetite MtTR-1 was nearly similar to that of natural magnetite. Electron probe microanalysis (EPMA) and LA-ICP-MS were conducted to analyze the minor and trace elements in MtTR-1, evaluate the homogeneity, and ICP-optical emission spectrometry (ICP-OES) and ICP-MS were used to report the reference values for 26 elements. MtTR-1 can be used as an in-house monitoring RM for LA-ICP-MS trace element analyses of magnetite. The proposed high-temperature and high-pressure preparation method for magnetite can also be applied to other minerals for in situ elemental analyses.

EXPERIMENTAL

Preparation of magnetite tablet. The initial material used for the synthesis was a magnetite RM from China [GBW (E) 010350]. The RM is commonly used as a monitoring sample to analyze the chemical composition of magnetite. GBW (E) 010350 RM has a grain size of <0.080 mm (180 mesh) and contained 13 elements with certified values (Table S1). The pressed magnetite tablets were prepared at the Key Laboratory for High Temperature and High Pressure Study of the Earth's Interior, Institute of Geochemistry, Chinese Academy of Sciences (IGCAS), Guiyang. The preparation process included grinding, magnetic separation, tableting, and high-pressure sintering. A high-energy vibration ball mill (F-VC100, Focucy, China) with a 50 mL agate vial was used to grind the initial magnetite powder to nanoscale particles. The wet grinding technique was used because it is more effective. After loading with 4 g of magnetite powder, 10 mL of anhydrous ethanol, and ~20 g of agate milling balls (8, 6, and 4 mm, 1:1:1 mass ratio), the agate vial was vacuumed and filled with high-purity argon (99.99%) to avoid oxidation of magnetite. Grinding was conducted at consecutive time intervals of 3 min with a 2 min interval for cooling, and the total grinding time was 4 h. Subsequently, the sample suspension was separated and collected in a Teflon PFA bottle, and wet magnetic separation was performed several times to remove most of the non-magnetic particles. After magnetic separation, the samples were dried in a vacuum oven at 60 °C for 4 h. The dried powder was re-homogenized manually for 5 min using an agate mortar and pestle. In the tableting step, the powder was pressed into a magnetite cylinder (10 mm in diameter and 9.2 mm in height) using a 10 mm tablet press at 2 t for 1 min. Subsequently, the magnetite cylinder was placed in a silver tube, which was then sealed by welding. The silver tube containing the magnetite cylinder was assembled into a high-pressure package, as shown in Fig. 1. High-pressure sintering was conducted at 500 °C and 1.2 GPa for 2 h using a cubic multi-anvil press.
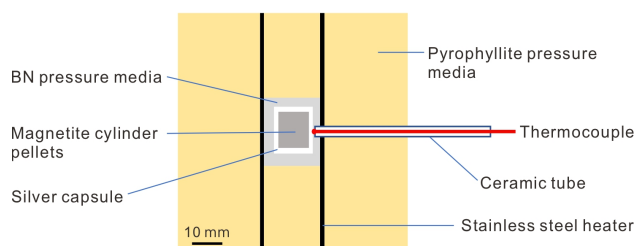
Fig. 1 Schematics of the high-pressure package.

Particle size and density analysis. Particle sizes of magnetite powders were determined by Beckman Coulter LS 13 320 particle size analyzer at the Center for Lunar and Planetary Sciences, IGCAS, using fifteen reading cycles with a cycle duration of 51 seconds. The density of the pressed pellet was determined by OLABO density balance (JA3003J) using Archimedes method.

Laser Raman spectroscopy (LRS). Before EPMA and LA-ICP-MS analyses, LRS was used to identify the MtTR-1 phase. The analysis was conducted at the State Key Laboratory of Ore Deposit Geochemistry (SKLODG), IGCAS, using LabRAM HR Evolution with an open space microscope equipped with a 20× objective (NA 0.25). The diameter of the laser spot was ~2 μm. A backscattering geometry was used in the 100–2000 cm^{-1} range with a 600 l.mm^{-1} grating. The Raman spectra were acquired using a 532 nm laser and a power of ~5 mW. Two consecutive acquisitions were obtained that lasted 20 s each.

Electron probe microanalysis. Major and minor elemental analyses of pressed magnetite were performed at the SKLODG, IGCAS, Guiyang, using a JEOL JXA8230 electron probe microanalyzer. Point analysis was conducted using a 5-μm diameter beam, a 25 kV voltage, and a current of 10 nA. The integration times for the element peak and background signal were 10 s and 5 s, respectively. Two sets of standards, natural and synthetic minerals (SPI #02753-AB; SPI Supplies, West Chester, USA) and metals (SPI #02751-AB), were used for quantifying the element concentration. The average detection limits were 67 μg g^{-1} for K; 92 μg g^{-1} for Ca; 140–180 μg g^{-1} for Fe, Mn, Cu, Zn, Cu, Al, Mg, P, and Ni; and 220–250 μg g^{-1} for Ti, Si, and Na.

LA-ICP-MS. Minor and trace elements of magnetite were determined using New Wave 213 nm and GeoLasPro 193 nm laser ablation systems coupled with an Agilent 7700x ICP-MS at the SKLODG, IGCAS, Guiyang. The operating conditions of the ICP-MS and laser ablation systems are listed in Table 1. Each analysis included a gas background acquisition of ~15 s and a 40 s sample signal acquisition. The spot sizes were set to 38, 44, 51, and 60 μm, and the repetition rate was 4 or 5 Hz. Every 10 sample analyses were followed by analyses of standards and monitoring samples. The elemental contents were calibrated against the iron-

Table 1. LA-ICP-MS operation conditions

	SKLODG1	SKLODG2	HFUT
ICP-MS	Agilent 7700x	Agilent 7700x	Agilent 7900
RF power	1350 W	1350 W	1350 W
Plasma gas	14 L min^{-1} Ar	14 L min^{-1} Ar	14 L min^{-1} Ar
Auxiliary gas	0.9 L min^{-1} Ar	0.9 L min^{-1} Ar	0.9 L min^{-1} Ar
Make-up gas	0.8 L min^{-1} Ar	0.8 L min^{-1} Ar	0.9 L min^{-1} Ar
Sampling depth	5 mm	5 mm	5.5 mm
Detector	Dual (pulse and analog counting)	Dual (pulse and analog counting)	Dual (pulse and analog counting)
Dwell time/mass	6 ms	6 ms	6 ms
Laser ablation system	New Wave NWR213	GeoLasPro 193 nm	Photon Machines Analyte HE
Wavelength	213 nm	193 nm	193 nm
Energy density	5 J cm^{-2}	5 J cm^{-2}	2.5 J cm^{-2}
Carrier gas	He	He	He
Ablation style	Single spot	Single spot	Line raster (scan rate 20 μm s^{-1})
Spot size	38 or 51 μm	44 or 60 μm	55 μm
Repetition rate	5 Hz	4 Hz	7 Hz
Laser pulse	200	160	1050

Note: SKLODG-State Key Laboratory of Ore Deposit Geochemistry, HFUT-Hefei University of Technology.

rich synthetic glass, GSE-1G, BCR-2G, BIR-1G, and BHVO-2G, using ^{57}Fe as the internal standard. Iron content was determined by EPMA. Synthetic glass, GOR-28G, and natural magmatic magnetite, BC-28, were used as monitoring samples. The results of the monitoring samples are listed in Table S2. Signal interval selection and content calibration were performed using the ICPMSDataCal software.[11] Line analysis across the magnetite sample was conducted at the In Situ Mineral Geochemistry Lab, Ore Deposit and Exploration Center, Hefei University of Technology, China. The equipment was composed of an Agilent 7900 Quadrupole ICP-MS coupled to a Photon Machines Analyte HE 193-nm ArF Excimer laser system. The operation condition is shown in Table 1.

ICP-OES and ICP-MS analyses. Major elements were determined by Agilent 720 ICP-OES, and trace elements were determined by Jena PlasmaQuant MS Elite ICP-MS, at the SKLODG, IGCAS, Guiyang. The analytical procedure can be found in Qi *et al*. (2000)[38] and was summarized here. Approximately 25 mg of magnetite powders were digested with a mixture of HNO$_3$ and HF in sealed PTFE bombs and heated to 190°C for 24 h in an electronic oven. After cooling, the sample solution was dried at 150°C on a hot plate. Rh solution (internal standard), de-ionized water and HNO$_3$ were added, and the bombs were resealed and heated to 145°C in an oven for 3 h. The final solution was taken out and diluted to two groups of solution which are suitable for ICP-MS and ICP-OES analyses, respectively. The multi-element standard solutions were used as external standard to calculate the element concentration. BCR-1 and GBPG-1 were used as monitoring samples during ICP-MS analysis, whereas GSR-3, BCR-1, BHVO-1, GSD-1, GSR-12, and GSR-13 were used as monitoring samples during ICP-OES analysis.
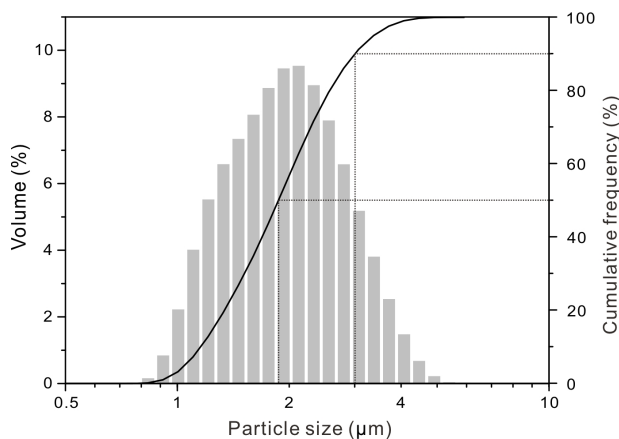
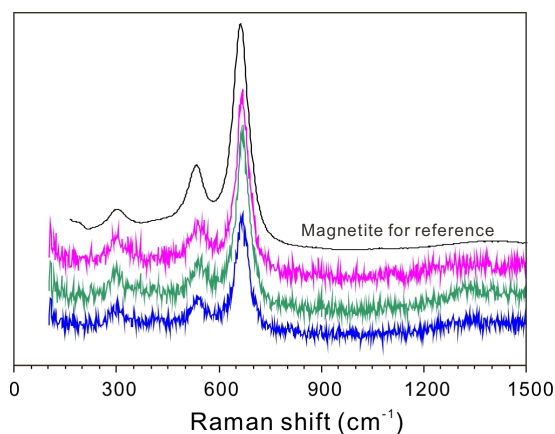**Fig. 2** Grain size distribution of magnetite powder after milling (d_{90} = 3.0 μm and d_{50} = 1.8 μm).

Fig. 3 Raman spectra of MtTR-1 and the standard magnetite from the RRUFF database (https://rruff.info/magnetite/display=default/R060191). Y-axis represents signal intensity (not scaled). Red, green, and blue lines represent three individual analyses.

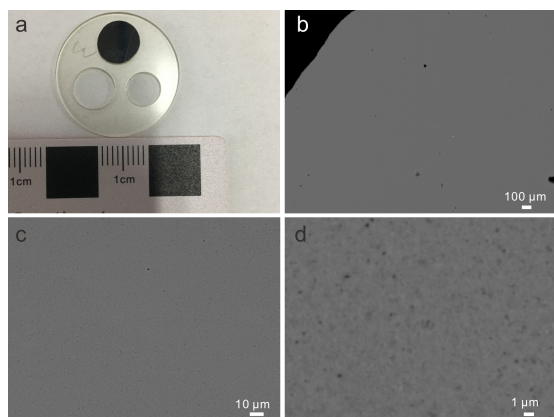**Fig. 4** (a) Slice of prepared magnetite (MtTR-1) with a diameter of ~1 cm. (b–c) Backscattered electronic (BSE) images at different scales showing the polished surface of MtTR-1. The surface is smooth with grain size on the nanometer scale. Some small holes in the top image (b) are caused due to polishing.

RESULTS AND DISCUSSION

Selection of conditions for sample preparation. To obtain submicron particles, experiments were conducted to select the milling ball size, number of balls, and ball-to-powder ratio.[20] It was observed that smaller milling balls can produce smaller particles. There were no obvious differences in homogeneity when subsequent milling was performed using 15 mm and 7 mm milling balls and 10 mm and 7 mm milling balls.[22] To avoid contamination during sample transfer, 7 mm milling balls were used with a ball-to-powder ratio of 17.[22] Here, one-step milling was performed using a mixture of 8 mm, 6 mm, and 4 mm milling balls to obtain nanoparticles. In order to obtain finer particle, the assemblage of 8 mm, 4 mm, and 2 mm milling balls was used, but 2 mm balls were lost after milling. Therefore, the assemblage of 8 mm, 6 mm, and 4 mm milling balls was preferred. Wet milling is more effective than dry milling, and ultrapure water was used in a previous study.[22] Anhydrous ethanol was used instead of water in the present study because it was easy to dry. The powder with grain size of d_{90} = 3.0 μm and d_{50} = 1.8 μm was obtained after optimizing the sample preparation conditions (Fig. 2). The grain size distribution result of magnetite powder was better than that (d_{90} = 4.8–22.8 μm and d_{50} = 1.3–2.3 μm) of basaltic and granitic rock powders after wet milling.[22] Because magnetite is magnetic, it was difficult to separate the particles during the particle size analysis. Therefore, the actual particle size may be lower than the measured values. Experimental studies have shown that magnetite can be stable at ~12 GPa between 300 and 1200 K (Fig. S1).[39,40] The increase of temperature can shorten the sintering time, but too high temperature may lead to sample decomposition, the loss of volatile elements, and the reaction between the sample and the coating material. Therefore, an intermediate temperature of 500 °C was chosen and only two hours are needed to sintering the sample. In addition, 1.2 GPa is chosen because magnetite is very stable at this pressure (Fig. S1). Moreover, this pressure can be easily achieved by the available high-pressure equipment, which is enough to eliminate the porosity between magnetite particles.

Phase identification of MtTR-1. To determine possible phase transition during grinding and high-temperature and high-pressure sintering, three spot analyses were performed using LRS at different locations on the pellet, from the core to the margin. MtTR-1 was identified by a strong band at 666 cm^{-1} by comparing it with the standard Raman spectrum of magnetite (Fig. 3). This indicates that magnetite was not transformed into other Fe oxides phases during sample preparation, even under high-temperature (500 °C) and high-pressure (1.2 GPa) conditions. This is consistent with the experimental and thermodynamic results for the iron-oxide phases. The transition of magnetite to a high-pressure h-Fe_3O_4 phase will occur under 27 GPa at both room temperature and 20 K (Fig. S1).[39] Magnetite can be transformed to hematite and wüstite at 298 K under a pressure of 13.3 GPa, and the stability field for the hematite and wüstite mixture narrows when

Table 2. Statistical summary of EPMA results of the prepared magnetite (MtTR-1)

Analysis no.	FeO wt%	MnO wt%	ZnO wt%	CuO wt%	TiO$_2$ wt%	SiO$_2$ wt%	Al$_2$O$_3$ wt%	Na$_2$O wt%	MgO wt%	K$_2$O wt%	P$_2$O$_5$ wt%	CaO wt%	NiO wt%	Total wt%
Average	86.8	0.072	0.035	0.028	0.059	2.25	0.248	0.077	0.636	0.014	0.047	0.156	0.028	90.3
Stdev	0.4	0.018	0.019	0.009	0.022	0.12	0.028	0.041	0.068	0.005	0.013	0.120	0.007	0.4
RSD (%)	0.5	24.6	54.2	32.4	36.8	5.4	11.4	53.7	10.7	32.5	28.3	77.2	24.0	0.4
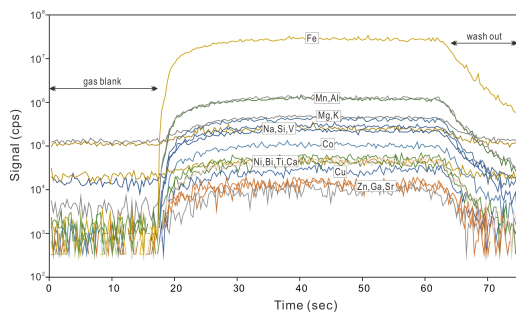
Fig. 5 Signal intensity of selected elements during LA-ICP-MS of MtTR-1 using a spot size of 51 μm. Very stable signals of the selected elements indicate their homogeneous distribution in magnetite depth profile. The relative standard deviation (RSD, %) for Fe, Mn, Al, Mg, K, Na, Si, V, Co, Ni, Bi, Ti, Ca, Cu, Zn, Ga, and Sr at the integration time between 30 and 60 s are 6%, 7%, 6%, 7%, 6%, 6%, 7%, 28%, 8%, 11%, 12%, 14%, 11%, 15%, 19%, 25%, and 22%, respectively.
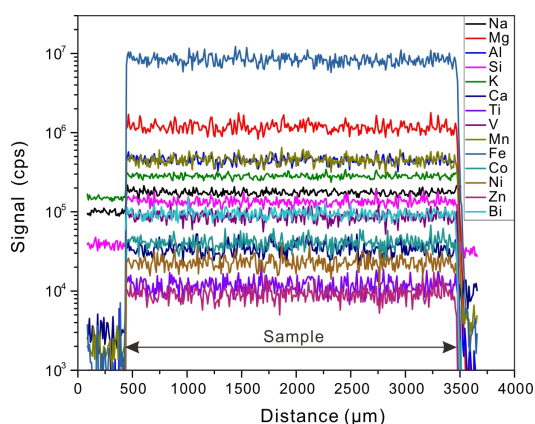
Fig. 6 A line profile showing the signal intensity during LA-ICP-MS line scanning analysis of magnetite. The relative standard deviation (RSD, %) for Na, Mg, Al, Si, K, Ca, Ti, V, Mn, Fe, Co, Ni, Zn, and Bi at the distance between 500 and 3400 μm are 7%, 14%, 11%, 11%, 6%, 18%, 21%, 14%, 13%, 14%, 17%, 18%, 19%, and 12%, respectively.

temperature increases, reaching a maximum temperature of ~850 K under a pressure 14.6 GPa (Fig. S1).[40]

Homogeneity of MtTR-1. The pressed magnetite had a density of 5.06 g cm^{-3}, which was similar to natural magnetite (5.1–5.2 g cm^{-3}, http://webmineral.com) and can be repeatedly polished for in situ analyses (Fig. 4a). The presence of impurities, such as Si and Mg, in pressed magnetite decreases the density. The polished

magnetite had a mirror-like surface, and the grain size of the magnetite was in the nanometer scale (Figs. 4b–d). In order to evaluate the homogeneity of MtTR-1, the pellet was cut into different pieces and two pieces were randomly selected for EPMA and LA-ICP-MS analyses. Because there are no differences in the results between two pieces for EPMA analyses, the results from two pieces are described together to obtain mean composition. The EPMA results showed that the concentrations of FeO, MnO, SiO$_2$, Al$_2$O$_3$, MgO, and CaO were above their respective detection limits (Table S3). However, the amount of data below the detection limits for ZnO, CuO, TiO$_2$, Na$_2$O, K$_2$O, P$_2$O$_5$, and NiO was 20, 13, 42, 34, 44, 6, and 20, respectively, for a total of 100 analyses. The relative standard deviations (RSD, n=100 analyses) for FeO, SiO$_2$, Al$_2$O$_3$, and MgO were 0.5, 5.4, 11.4, and 10.7%, respectively (Table 2), which is comparable to the EPMA analytical precision, indicating a homogeneous composition of the pressed magnetite at 5-μm spatial resolution. Other elements showed larger RSD because their concentrations were lower than 0.1 wt%.

The homogeneity of MtTR-1 was verified using LA-ICP-MS. Fig. 5 shows the time-resolved signal spectrum of elements with signal intensities higher than 1000 cps. Elements, including Fe, Mn, Al, Mg, K, Na, Si, V, Co, Ni, Bi, Ti, and Ca, showed very stable signals without obvious peaks or valleys (Fig. 5). Elements such as Cu, Zn, Ga, and Sr showed slight fluctuations in signals; however, the variations were within 2σ uncertainties (Fig. 5) and were thus considered being homogeneous in magnetite as the spatial resolution of LA-ICP-MS. In addition, an ~3 mm profile across the MtTR-1 sample also demonstrated good homogeneity for the selected elements (Fig. 6). Because no signal homogenizing equipment was used between the laser ablation and ICP-MS equipment, the ICP-MS signals of elements represent the real-time conditions during laser ablation, aerosol transport, and mass spectrometry analysis. Any signal anomaly could be recognized easily. The morphologies of the ablation craters at spot size 38 and 51 μm were slightly different. The 38 μm crater was circular, whereas the 51 μm carter was oval (Fig. 7). The slightly different shape and morphology of ablation craters produced by 38 and 51 μm-spot size are possibly related to laser properties (e.g., beam profile). The ablation craters of MtTR-1 at the two spot sizes showed steep walls and smooth bottoms (Fig. 7) and were similar to those of natural sample[41] and nanoparticulate PPT.[22]

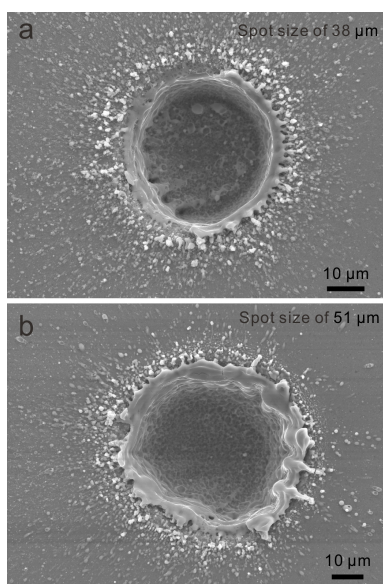**Preferred values of MtTR-1.** In situ analytical methods,

Fig. 7 BSE image showing the laser ablation crater of MtTR-1 at spot sizes of 38 μm (a) and 51 μm (b) (ablation with 200 pulses obtained at 5 Hz and 5 J cm^{-2}). Note the crater walls and bottom are smooth. The sputter materials are homogeneous and composed of nanometer to micron-scale grains.
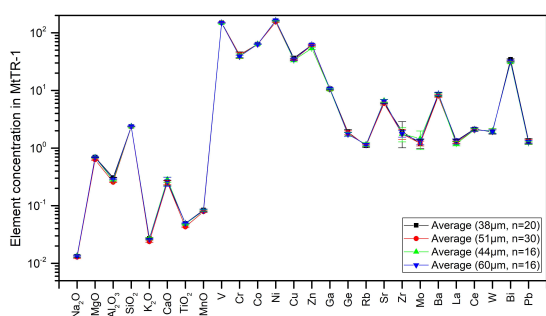

Fig. 8 LA-ICP-MS results of MtTR-1 at the spot sizes of 38, 44, 51, and 60 μm. The concentrations of elements expressed as oxides are in wt%, whereas the concentrations of other elements are in μg g^{-1}. The uncertainty for each element is 1σ.
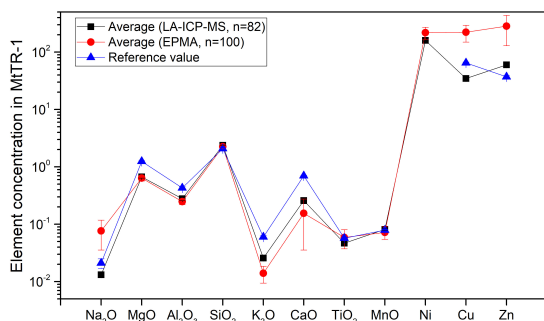

Fig. 9 EPMA and LA-ICP-MS results are compared with the reference values of initial powders from GBW(E)010350. The concentrations of oxides are in wt%, whereas the concentrations of Ni, Cu, and Zn are in μg g^{-1}. The uncertainty is 1σ.
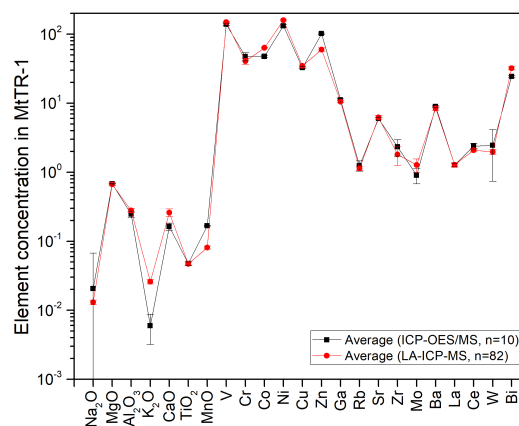

Fig. 10 Comparison between LA-ICP-MS and ICP-OES/MS results. The concentrations of elements expressed as oxides are in wt%, whereas the concentrations of other elements are in μg g^{-1}. The uncertainty for each element is 1σ.

including EPMA and LA-ICP-MS, were used to determine the concentrations of major and trace elements in MtTR-1. The summary of LA-ICP-MS results are listed in Table 3 and individual analyses can be found in Tables S4. Different spot sizes with different laser ablation systems yield similar results (Fig. 8), indicating that the ablation spot size had a negligible effect on the analytical results. By comparing the EPMA and LA-ICP-MS results, it was observed that the concentrations of Mg, Al, Si, Ca, Ti, Mn, and Ni were consistent within the uncertainty (Fig. 9). However, the results of Na, Cu, and Zn determined using EPMA were higher than those determined using LA-ICP-MS (Fig. 9). The inconsistent results for these elements may be due to the different detection limits of the two analytical methods. Because there were 34, 13, and 20 censored data (data below detection limit) points for Na, Cu, and Zn, respectively, in 100 EPMA results, the average concentrations of these elements after removing the censored data will be higher than the real values.

To investigate the potential variations in the chemical composition of magnetite tablet during sample preparation, the LA-ICP-MS data were compared with the reference values of the initial powders from GBW(E)010350. The concentrations of Si, Ti, and Mn determined using LA-ICP-MS were consistent with their respective reference values (Fig. 9). Because the magnetite sample was ground using an agate vial and milling balls, the expected contaminant was Si. However, the consistent results for Si among the EPMA, LA-ICP-MS, and reference values indicate that no additional Si was added, or contaminated SiO$_2$ nanoparticles was removed by magnetic separation after grinding. The concentrations of other elements, such as Na, Mg, Al, K, and Ca, determined using LA-ICP-MS were lower than the reference values, indicating that these impurities in magnetite were removed after sample preparation. This is consistent with the stable and smooth signal in the time-resolved LA-ICP-MS spectrum of these

Table 3. Statistical summary of LA-ICP-MS results of MtTR-1

	Na₂O	MgO	Al₂O₃	SiO₂	K₂O	CaO	TiO₂	MnO	V	Cr	Co	Ni	Cu	Zn	Ga	Ge	Rb	Sr	Zr	Mo	Ba	La	Ce	W	Bi	Pb
	wt%	wt%	wt%	wt%	wt%	wt%	wt%	wt%	µg g⁻¹	µg g⁻¹	µg g⁻¹	µg g⁻¹	µg g⁻¹	µg g⁻¹	µg g⁻¹	µg g⁻¹	µg g⁻¹	µg g⁻¹	µg g⁻¹	µg g⁻¹	µg g⁻¹	µg g⁻¹	µg g⁻¹	µg g⁻¹	µg g⁻¹	µg g⁻¹
SKLODG1																										
Average (38µm, n=20)	0.013	0.699	0.308	2.374	0.027	0.249	0.049	0.084	149.8	41.6	63.8	162.6	36.6	61.8	10.8	1.90	1.10	6.07	1.95	1.20	8.50	1.35	2.14	1.91	34.7	1.35
Stdev	0.001	0.013	0.004	0.033	0.001	0.026	0.001	0.003	1.2	5.0	1.1	2.8	2.8	1.9	0.3	0.20	0.07	0.20	0.93	0.22	0.72	0.06	0.09	0.16	0.8	0.12
Average (51µm, n=30)	0.013	0.630	0.256	2.367	0.024	0.252	0.043	0.079	149.3	41.1	63.2	154.1	34.1	60.7	10.4	1.85	1.12	5.93	1.77	1.21	8.01	1.27	2.05	1.99	31.1	1.29
Stdev	0.001	0.016	0.002	0.039	0.001	0.019	0.001	0.003	1.6	4.7	0.6	3.7	1.1	2.2	0.4	0.15	0.05	0.34	0.36	0.12	0.48	0.06	0.09	0.19	1.1	0.12
SKLODG2																										
Average (44µm, n=16)	0.013	0.691	0.276	2.376	0.027	0.284	0.048	0.082	147.9	39.5	63.6	161.7	33.6	53.7	10.4	1.73	1.16	6.62	1.77	1.46	8.57	1.20	2.06	2.00	30.9	1.24
Stdev	0.000	0.015	0.005	0.045	0.001	0.029	0.001	0.003	2.3	3.7	0.9	2.5	2.3	2.4	0.3	0.13	0.09	0.39	0.48	0.52	0.43	0.10	0.11	0.19	0.8	0.08
Average (60µm, n=16)	0.013	0.690	0.292	2.388	0.026	0.264	0.049	0.082	148.5	38.9	63.3	164.1	34.7	62.1	10.8	1.75	1.14	6.49	1.78	1.30	8.80	1.31	2.11	1.94	32.3	1.28
Stdev	0.000	0.011	0.009	0.041	0.001	0.047	0.001	0.005	1.5	1.8	0.9	3.2	1.1	1.8	0.3	0.14	0.05	0.44	0.23	0.15	0.52	0.14	0.16	0.14	1.1	0.09
Average (all data, n=82)	0.013	0.670	0.279	2.374	0.026	0.260	0.047	0.081	149.0	40.5	63.5	159.6	34.7	59.9	10.5	1.82	1.13	6.21	1.81	1.27	8.39	1.28	2.09	1.97	32.1	1.29
Stdev	0.001	0.034	0.021	0.039	0.002	0.032	0.003	0.004	1.8	4.3	0.9	5.3	2.2	3.7	0.4	0.17	0.07	0.44	0.56	0.28	0.62	0.10	0.12	0.17	1.8	0.11

Table 4. Statistical summary of ICP-OES and ICP-MS results of MtTR-1

	Na₂O	MgO	Al₂O₃	K₂O	CaO	TiO₂	MnO	V	Cr	Co	Ni	Cu	Zn	Ga	Rb	Sr	Zr	Mo	Ba	La	Ce	W	Bi
	wt%	wt%	wt%	wt%	wt%	wt%	wt%	µg g⁻¹	µg g⁻¹	µg g⁻¹	µg g⁻¹	µg g⁻¹	µg g⁻¹	µg g⁻¹	µg g⁻¹	µg g⁻¹	µg g⁻¹	µg g⁻¹	µg g⁻¹	µg g⁻¹	µg g⁻¹	µg g⁻¹	µg g⁻¹
Average (n=10)	0.021	0.68	0.25	0.006	0.163	0.047	0.167	139	47.3	47.6	132.0	32.6	101	11.2	1.25	5.98	2.33	0.90	8.97	1.27	2.39	2.44	24.40
Stdev	0.047	0.01	0.03	0.003	0.019	0.002	0.002	4.5	6.5	1.6	5.1	1.1	3	0.3	0.21	0.21	0.63	0.22	0.33	0.08	0.24	1.70	0.57

Note: Major oxides are determined by ICP-OES, whereas other elements are determined by ICP-MS.

elements, which precludes the existence of micron-scale mineral inclusions (Figs. 5 and 6).

Solution ICP-OES and ICP-MS were used to determine the contents of major and trace elements in MtTR-1. A total of 23 elements were analyzed, the full results can be found in Table S5 and the statistical summary is shown in Table 4. These values are used as the preferred values for MtTR-1. The contents of MgO, Al₂O₃, and CaO obtained by EPMA are consistent with those of the solution ICP-OES results with uncertainties (Tables 2 and 4), indicating the reliability of EPMA results. Because Si and Fe are not analyzed by ICP-MS/OES, EPMA Si and Fe contents can be used as preferred values. By comparing the LA-ICP-MS results with ICP-MS/OES, it is shown that Mg, Al, Ti, V, Cr, Ni, Cu, Ga, Rb, Sr, Zr, Mo, Ba, La, Ce, and W contents are consistent for these techniques (Fig. 10). This indicates that LA-ICP-MS method for determination of trace elements in magnetite is reliable. However, the contents of some elements including K, Na, Mn, Co, Ni, and Zn determined by LA-ICP-MS are inconsistent with those obtained by ICP-MS/OES. The reason remains unknown, which may be related to element behavior during laser ablation or matrix effect. Further work is needed to solve this issue.

Main merits of high-temperature and high-pressure sintering technique. Compared to pressed pellet produced under room temperature and relatively low pressure (*e.g.*, several to hundreds of MPa), the high-temperature and high-pressure sintering technique has the following advantages. First, the density of pressed pellet is close to natural mineral, so that it is not easy to break. Due to high density and low porosity, the surface and interior of the pressed pellet are not easily oxidized when exposed in the air. No vacuum environment is needed to store the standard. Second, there are no differences in color and density between pressed pellet with sintering and natural mineral, and thus light absorption behavior is similar during LA-ICP-MS analysis. Similar color, density, and chemical composition between pressed pellet and natural mineral meet the requirement of matrix matching. Third, the pressed pellet can be cut into different pieces and shared with other laboratories. Moreover, the pellet can be repeatedly polished to get a mirror-like surface like synthesized glass standard and thus can meet numerous LA-ICP-MS analyses.

CONCLUSION

In this study, we developed a new technique for preparing pressed magnetite tablets for *in situ* microanalysis. Primary magnetite powder with a grain size of ~80 μm was milled to approximately <3 μm under wet conditions using anhydrous ethanol as the medium. The powders were pressed into tablets under 500 °C and 1.2 GPa without adding a binder. The magnetite tablet had a density that was nearly similar to that of natural magnetite with a homogeneous trace element composition, as demonstrated by EPMA (spot size of 5 μm) and LA-ICP-MS (spot sizes of 38-60 μm) results. The contents of twenty-three elements determined by ICP-OES/MS are used as preferred values. The magnetite tablet was cut into slices, polished, and used repeatedly. Our study demonstrated that high-temperature and high-pressure methods are efficacious for preparing homogeneous PPT for in situ elemental analysis and potentially isotopic ratio analyses, which are superior to natural magnetite RMs.

ASSOCIATED CONTENT

The supporting information (Tables S1−S5 and Fig. S1) is available at www.at-spectrose.com/as/home.

AUTHOR INFORMATION
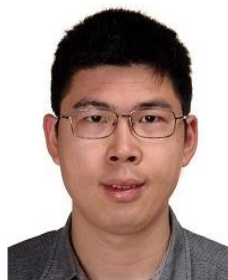
Sen Lin received his PhD in 2013 from the Institute of Geochemistry, Chinese Academy of Sciences (CAS). He is an associate professor of geochemistry at the Institute of Geochemistry, CAS. His major research interests are high pressure science and technology, hydrothermal geochemistry and their applications to geochemistry of ore deposit. He is currently working on development of reference materials for in situ microanalysis such as LA-ICP-MS and nano-SIMS.

Corresponding Author

* S. Lin

Email address: linsen@mail.gyig.ac.cn

Notes

The authors declare no competing financial interest.

ACKNOWLEDGMENTS

REFERENCES

1. P. Nadoll, T. Angerer, J. L. Mauk, D. French, and J. Walshe, *Ore Geol. Rev.*, 2014, **61**, 1–32. https://doi.org/10.1016/j.oregeorev.2013.12.013

2. C. Dupuis and G. Beaudoin, *Miner. Deposita*, 2011, **46**, 319–335. https://doi.org/10.1007/s00126-011-0334-y

3. S. A. S. Dare, S.-J. Barnes, G. Beaudoin, J. Méric, E. Boutroy, and C. Potvin-Doucet, *Miner. Deposita*, 2014, **49**. 785–796. https://doi.org/10.1007/s00126-014-0529-0

4. X.-W. Huang, A.-A. Sappin, É. Boutroy, G. Beaudoin, and S. Makvandi, *Econ. Geol.*, 2019, **114**, 917–952. https://doi.org/10.5382/econgeo.4648

5. N. Cook, C. L. Ciobanu, L. George, Z.-Y. Zhu, B. Wade, and K. Ehrig, *Minerals*, 2016, **6**, 1–34. https://doi.org/10.3390/min6040111

6. Y. Liu, Z. Hu, M. Li, and S. Gao, *Chin. Sci. Bull.*, 2013, **58**, 3863–3878. https://doi.org/10.1007/s11434-013-5901-4

7. S. E. Jackson, H. P. Longerich, G. R. Dunning, and B. J. Fryer, *Can. Mineral.*, 1992, **30**, 1049–1064.

8. P. Nadoll and A. E. Koenig, *J. Anal. At. Spectrom.*, 2011, **26**, 1872–1877. https://doi.org/10.1039/C1JA10105F

9. D. X. Zhang, T. G. Dai, and Y. Hu, *Rock Miner. Anal.*, 2012, **31**, 120–126. https://doi.org/10.3969/j.issn.0254-5357.2012.01.015

10. D. Savard, S. J. Barnes, S. Dare, and G. Beaudoin, *Mineral. Mag.*, 2012, **76**, 2329.

11. Y. Liu, Z. Hu, S. Gao, D. Günther, J. Xu, C. Gao, and H. Chen, *Chem. Geol.*, 2008, **257**, 34–43. https://doi.org/10.1016/j.chemgeo.2008.08.004

12. J.-F. Gao, M.-F. Zhou, P. C. LightFoot, C. Y. Wang, L. Qi, and M. Sun, *Econ. Geol.*, 2013, **108**, 1833–1848. https://doi.org/10.2113/econgeo.108.8.1833

13. X.-W. Huang, M.-F. Zhou, L. Qi, J.-F. Gao, and Y.-W. Wang, *Miner. Deposita*, 2013, **48**, 925–946. https://doi.org/10.1007/s00126-013-0467-2

14. Y.-M. Meng, X.-W. Huang, J.-F. Gao, Z.-H. Dai, and L. Qi, *Rock Miner. Anal.*, 2016, **35**, 585–594. https://doi.org/10.15898/j.cnki.11-2131/td.2016.06.004

15. S. Wu, Y. Yang, K. P. Jochum, R. L. Romer, J. Glodny, I. P. Savov, S. Agostini, J. C. M. De Hoog, S. T. M. Peters, A. Kronz, C. Zhang, Z. Bao, X. Wang, Y.Li, G. Tang, L. Feng, H. Yu, Z. Li, L. Zhang, J. Lin, Y. Zeng, C. Xu, Y. Wang, Z. Cui, L. Deng, J. Xiao, Y. Liu, D. Xue, D. Zhang, L. Jia, H. Wang, L. Xu, C. Huang, L. Xie, A. Pack, G. Wörner, M. He, C. Li, H. Yuan, F. Huang, Q. Li, J. Yang, X. Li, and F. Wu, *Geostand. Geoanal. Res.*, 2021, **45**, 719–745. https://doi.org/10.1111/ggr.12399

16. S. Wu, G. Wörner, K. P. Jochum, B. Stoll, K. Simon, and A. Kronz, *Geostand. Geoanal. Res.*, 2019, **43**, 567–584. https://doi.org/10.1111/ggr.12301

17. P. V. S. Raju, S.-J. Barnes, and D. Savard, in *11th International Platinum Symposium*. 2010.

18. S. A. S. Dare, S.-J. Barnes, and G. Beaudoin, *Geochim. Cosmochim. Acta*, 2012, **88**, 27–50. https://doi.org/10.1016/j.gca.2012.04.032

19. L.-M. Chen, X.-Y. Song, R.-Z. Hu, S.-Y. Yu, H.-L. He, Z.-H. Dai, Y.-W. She, and W. Xie, *Am. Mineral.*, 2017, **102**, 1006–1020. https://doi.org/10.2138/am-2017-5804

20. N. K. Saini, P. K. Mukherjee, M. S. Rathi, and P. P. Khanna, *X-Ray Spectrom.*, 2000, **29**, 166–172.

21. https://doi.org/10.1002/(SICI)1097-4539(200003/04)29:2<166::AID-XRS411>3.0.CO;2-L

21. A. L. Gray, *Analyst*, 1985, **110**, 551–556. https://doi.org/10.1039/AN9851000551

22. D. Garbe-Schönberg and S. Müller, *J. Anal. At. Spectrom.*, 2014, **29**, 990–1000. https://doi.org/10.1039/C4JA00007B

23. P. K. Mukherjee, P. P. Khanna, and N. K. Saini, *Geostand. Geoanal. Res.*, 2014, **38**, 363–379. https://doi.org/10.1111/j.1751-908X.2013.00260.x

24. S. Wu, V. Karius, B. C. Schmidt, K. Simon, and G. Wörner, *Geostand. Geoanal. Res.*, 2018, **42**, 575–591. https://doi.org/10.1111/ggr.12230

25. K. P. Jochum, D. Garbe-Schönberg, M. Veter, B. Stoll, U. Weis, M. Weber, F. Lugli, A. Jentzen, R. Schiebel, and J. A. Wassenburg, *Geostand. Geoanal. Res.*, 2019, **43**, 595–609. https://doi.org/10.1111/ggr.12292

26. S. T. Wu, C. X. Xu, Z. D. Chen, Y. P. Wang, and J. F. Bai, *Chin. J. Analy. Lab.*, 2019, **38**, 1089–1094. https://doi.org/10.13595/j.cnki.issn1000-0720.2018.110102

27. P. Onuk, F. Melcher, R. Mertz-Kraus, H.-E. Gäbler, and S. Goldmann, *Geostand. Geoanal. Res.*, 2017, **41**, 263–272. https://doi.org/10.1111/ggr.12154

28. C. C. Wohlgemuth-Ueberwasser, C. Ballhaus, J. Berndt, V. S. Paliulionyte, and T. Meisel, *Contrib. Mineral. Petrol.*, 2007, **154**, 607–617. https://doi.org/10.1007/s00410-007-0212-x

29. Y. Lin, L. Feng, J. Hao, Y. Liu, S. Hu, J. Zhang, and W. Yang, *J. Anal. At. Spectrom.*, 2014, **29**, 1686–1691. http://dx.doi.org/10.1039/C4JA00136B

30. A. A. Van Heuzen and J. B. W. Morsink, *Spectrochim. Acta B*, 1991, **46**, 1819–1828. https://doi.org/10.1016/0584-8547(91)80208-K

31. A. Stankova, N. Gilon, L. Dutruch, and V. Kanicky, *J. Anal. At. Spectrom.*, 2011, **26**, 443–449. https://doi.org/10.1039/C0JA00020E

32. C. O'Connor, M. R. Landon, and B. L. Sharp, *J. Anal. At. Spectrom.*, 2007, **22**, 273–282. https://doi.org/10.1039/B612512C

33. M. E. Shaheen and B. J. Fryer, *Spectrochim. Acta B*, 2011, **66**, 627–636. https://doi.org/10.1016/j.sab.2011.06.010

34. Y. Zhu, A. Hioki, and K. Chiba, *J. Anal. At. Spectrom.*, 2013, **28**, 301–306. https://doi.org/10.1039/C2JA30279A

35. M. Pakieła, M. Wojciechowski, B. Wagner, and E. Bulska, *J. Anal. At. Spectrom.*, 2011, **26**, 1539–1543. https://doi.org/10.1039/C0JA00201A

36. N. Imai, *Anal. Chim. Acta*, 1990, **235**, 381–391. https://doi.org/10.1016/S0003-2670(00)82097-8

37. M. Motelica-Heino, O. F. X. Donard, and J. M. Mermet, *J. Anal. At. Spectrom.*, 1999, **14**, 675–682. https://doi.org/10.1039/A808088G

38. L. Qi, J. Hu, and D. C. Gregoire, *Talanta*, 2000, **51**, 507–513. https://doi.org/10.1016/S0039-9140(99)00318-5

39. K. Chen, F. Baudelet, Y. Mijiti, L. Nataf, A. Di Cicco, Z. Hu, S. Agrestini, A. C. Komarek, M. Sougrati, J. Haines, J. Rouquette, Q. Kong, and T.-C. Weng, *J. Phys. Chem. C*, 2019, **123**, 21114–21119. https://doi.org/10.1021/acs.jpcc.9b04140

40. P. Lazor, O. N. Shebanova, and H. Annersten, *J. Geophys. Res.*, 2004, **109**, 1–16. https://doi.org/10.1029/2003JB002600

41. S. E. Gilbert, L. V. Danyushevsky, K. Goemann, and D. Death, *J. Anal. At. Spectrom.*, 2014, **29**, 1024–1033. https://doi.org/10.1039/C4JA00012A